MULTISCALE MODEL. SIMUL.
Vol. 16, No. 3, pp. 1448–1453

ERRATUM: THE INTERPLAY OF CURVATURE AND VORTICES IN FLOW ON CURVED SURFACES*

SEBASTIAN REUTHER† AND AXEL VOIGT‡

Abstract. We here correct the model and the derivation of the vorticity-stream function formulation for the incompressible surface Navier–Stokes equation on moving surfaces, proposed in [S. Reuther and A. Voigt, *Multiscale Model. Simul.*, 13 (2015), pp. 632–643].

Key words. curved surfaces, geometric force, interface

AMS subject classifications. 35Q35, 76D17, 53Z05, 14Q10

DOI. 10.1137/18M1176464

In [6] the vorticity-stream function formulation for an incompressible surface Navier–Stokes equation, introduced in [5], was extended to surfaces with a prescribed normal velocity. As the underlying Navier–Stokes equation the model proposed by Arroyo and DeSimone [1] was used. A more detailed derivation of the equation in [9] shows that the acceleration term in this model has to be corrected (cf. [9, Remark 2.3]). In the notation of [6] the tangential balance of linear momentum (equation (4.1) in [6]) should read

$$\partial_t \mathbf{v} + 2v_n \mathbf{S}\mathbf{v} - v_n \nabla_\Gamma v_n + \mathbf{v} \cdot \nabla_\Gamma \mathbf{v} = -\nabla_\Gamma p + \mu \left(\Delta_\Gamma^R \mathbf{v} + 2K\mathbf{v} - \nabla_\Gamma \left(v_n H \right) \right) + 2\mu \nabla_\Gamma \cdot \left(v_n \mathbf{S} \right),$$

with tangential velocity $\mathbf{v} = (v_1, v_2)$ with components corresponding to the local basis vectors $\mathbf{e}_1(\mathbf{x})$ and $\mathbf{e}_2(\mathbf{x})$ for each $\mathbf{x}$ on the evolving surface $\Gamma(t)$. The other quantities are pressure p, surface viscosity μ, shape operator $\mathbf{S}$, Gaussian curvature K, mean curvature H, and normal velocity v_n. Together with mass conservation (equation (4.2) in [6])

$$\nabla_\Gamma \cdot \mathbf{v} + v_n H = 0,$$

this gives the correct form for an incompressible surface Navier–Stokes equation on a prescribed surface which moves in normal direction with velocity v_n [9]. In the meantime other approaches to derive the incompressible Navier–Stokes equations on evolving surfaces have been proposed, in [3, 2] by using a variational principle and in [4] by using a thin shell limit. However, these approaches consider a three-dimensional surface velocity field $\mathbf{u}$ in Cartesian coordinates. Following [2] and considering the decomposition $\mathbf{u} = \mathbf{u}_T + v_n \mathbf{n}$ in tangential and normal components with $\mathbf{n}$ being the normal vector, an equation for $\mathbf{u}_T$ is derived (equation (3.12) in [2]). Considering our

*Received by the editors March 20, 2018; accepted for publication (in revised form) July 3, 2018; published electronically September 27, 2018.
http://www.siam.org/journals/mms/16-3/M117646.html
†Institute of Scientific Computing, Technische Universität Dresden, Dresden, Germany (sebastian.reuther@tu-dresden.de).
‡Institute of Scientific Computing, Technische Universität Dresden, Dresden Center for Computational Materials Science (DCMS), and Center for Systems Biology Dresden (CSBD), Dresden, Germany (axel.voigt@tu-dresden.de).

general model above in the embedding three-dimensional space with $\mathbf{v}_3 = (v_1, v_2, 0)$, extending all its components constantly in the normal direction and transforming it to Cartesian coordinates leads exactly to this model with a prescribed normal velocity v_n. To achieve this identity one has to deal with the delicate definition of the time derivative, which lacks tangentiality and tensorial properties; $\partial_t \mathbf{v}_3$ thereby transforms to $\mathbf{P}\partial_t \mathbf{u}_T - v_n \mathbf{S}\mathbf{u}_T$, where $\mathbf{P}$ is the orthogonal projection onto the tangent space. The corrected formulation and the established identity between the general model above and the three-dimensional models in Cartesian coordinates in [3, 2, 4] should end the controversial discussion on a proper definition for flow problems on evolving surfaces.

Not only the model in [6] has to be corrected but also the derivation of the vorticity-stream function formulation. It turns out that in the present setting the substitution $\mathbf{v}_3 = \mathrm{curl}\psi + \nabla_\Gamma \Phi$, with stream function ψ and potential Φ, leads to a more rigorous approach. Inserting this into the mass conservation law gives $\Delta_\Gamma \Phi + v_n H = 0$, an equation for Φ. The equations for the stream function ψ and the vorticity ϕ result from applying the curl $(\cdot)$ operator to the above momentum balance equation. In contrast to the assumption in [6] the curl operator curl $(\cdot)$ and the partial time derivative ∂_t are noncommuting operators, in general $\mathrm{curl}\,(\partial_t \mathbf{v}_3) \neq \partial_t \mathrm{curl}\,(\mathbf{v}_3)$. The correct identity is

$$\mathrm{curl}\,(\partial_t \mathbf{v}_3) = \partial_t \mathrm{curl}\,(\mathbf{v}_3) - v_n \mathbf{S} : \nabla_\Gamma\,(\mathbf{n} \times \mathbf{v}_3) - \mathrm{curl}(v_n) \cdot \mathbf{S}\mathbf{v}_3.$$

The complete system of scalar surface PDEs for the stream function ψ, the vorticity ϕ, and the potential Φ thus reads

$$\begin{aligned}
&\partial_t \phi + v_n \nabla_\Gamma \cdot (\mathbf{S}\,(\nabla_\Gamma \psi - \mathrm{curl}(\Phi))) + v_n J(H, \Phi) + v_n \nabla_\Gamma H \cdot \nabla_\Gamma \psi \\
&\quad - \mathrm{curl}\,(v_n) \cdot \mathbf{S}\,(\mathrm{curl}(\psi) + \nabla_\Gamma \Phi) + \mathrm{curl}\,(v_n \mathbf{S}\,(\mathrm{curl}(\psi) + \nabla_\Gamma \Phi)) \\
&\quad + J(\psi, \phi) + \nabla_\Gamma \cdot (\phi \nabla_\Gamma \Phi) \\
&\qquad = \mu\,(\Delta_\Gamma \phi + 2\nabla_\Gamma \cdot (K \nabla_\Gamma \psi) + 2J(K, \Phi) - 2\nabla_\Gamma \cdot (\mathbf{n} \times \nabla_\Gamma \cdot (v_n \mathbf{S}))) \\
&\qquad \phi = \Delta_\Gamma \psi \\
&-\Delta_\Gamma \Phi = v_n H.
\end{aligned}$$

Discretization. We first solve in each timestep the equation for the potential Φ^m, with index m denoting the new time, and afterward the equations for the stream function ψ^m and the vorticity ϕ^m. The finite element approximation thus reads as follows: Find $\Phi^m \in V_h^m$ such that for all $\gamma \in V_h^m$

$$\Big(\nabla_\Gamma \Phi^m \ ,\ \nabla_\Gamma \gamma\Big) = \Big(v_n H \ ,\ \gamma\Big).$$

Furthermore, find $(\phi^m, \psi^m) \in V_h^m \times V_h^m$ such that for all $(\alpha, \beta) \in V_h^m \times V_h^m$

$$\begin{aligned}
\Big(d_\tau \phi^m + \mathbf{p} \cdot \nabla_\Gamma \psi^m + J(\psi^{m-1}, \phi^m) \ ,\ \alpha\Big) &= \mu\Big(-\nabla_\Gamma \phi^m - 2K\nabla_\Gamma \psi^m \ ,\ \nabla_\Gamma \alpha\Big) \\
&\quad + \Big(\mathbf{M}\nabla_\Gamma \psi^m + \phi^m \nabla_\Gamma \Phi^m \ ,\ \nabla_\Gamma \alpha\Big) \\
&\quad + \Big(g \ ,\ \alpha\Big) + \Big(\mathbf{q} \ ,\ \nabla_\Gamma \alpha\Big) \\
\Big(\phi^m \ ,\ \beta\Big) &= -\Big(\nabla_\Gamma \psi^m \ ,\ \nabla_\Gamma \beta\Big)
\end{aligned}$$

with discrete time derivative d_τ and coefficient terms

$$\begin{aligned}
\mathbf{M} &:= v_n \left(\mathbf{S} + \mathbf{n} \times \mathrm{Curl}(\mathbf{n})^T\right), \\
\mathbf{p} &:= v_n \nabla_\Gamma H - \mathbf{S}\nabla_\Gamma v_n + \mathrm{Curl}(\mathbf{n})\mathrm{curl}(v_n), \\
\mathbf{q} &:= 2\mu \mathbf{n} \times \nabla_\Gamma \cdot (v_n \mathbf{S}) + v_n \mathbf{J}(\mathbf{n}, \Phi^m) - v_n \mathbf{n} \times (\mathbf{S}\nabla_\Gamma \Phi^m), \\
g &:= \nabla_\Gamma \Phi^m \cdot \mathbf{S}\mathrm{curl}\,(v_n) - v_n J(H, \Phi^m) + \mathbf{J}(\mathbf{n}, \Phi^m) \cdot \nabla_\Gamma v_n + 2\mu J(K, \Phi^m)
\end{aligned}$$

with a generalized cross product $\mathbf{n} \times \mathbf{A}$ with a matrix $\mathbf{A}$ and components $[\mathbf{n} \times \mathbf{A}]_{ij} := (\mathbf{n} \times \mathbf{A}\mathbf{e}_j)_i$, where $\mathbf{e}_j$ is the jth unit vector, another curl operator $\mathrm{Curl}(\mathbf{n})$ with components $[\mathrm{Curl}(\mathbf{n})]_{ij} = (\mathrm{curl}(\mathbf{n}_j))_i$, and the generalized Jacobian $\mathbf{J}(\mathbf{n}, \cdot)$ with components $[\mathbf{J}(\mathbf{n}, \cdot)]_i = J(\mathbf{n}_i, \cdot)$. The implementation is again done in the adaptive finite element toolbox AMDiS [7, 8].

Results. The simulation results shown in Figures 4–8 in [6] are reproduced with the corrected approach. The results are shown in Figures 4–8, respectively. In contrast to [6] we consider the tangential velocity $\mathbf{v}$ for visualization to also incorporate effects induced by the potential Φ. All numerical simulations show qualitatively the same and quantitatively very similar results. Small differences can be seen in Figures 7 and 8, where the vortex stays within the Gaussian saddle for longer times and the transition between equal and different vortex centers and saddle locations seems to be more linear, respectively. Both effects indicate an even tighter coupling between geometric properties and flow dynamics.

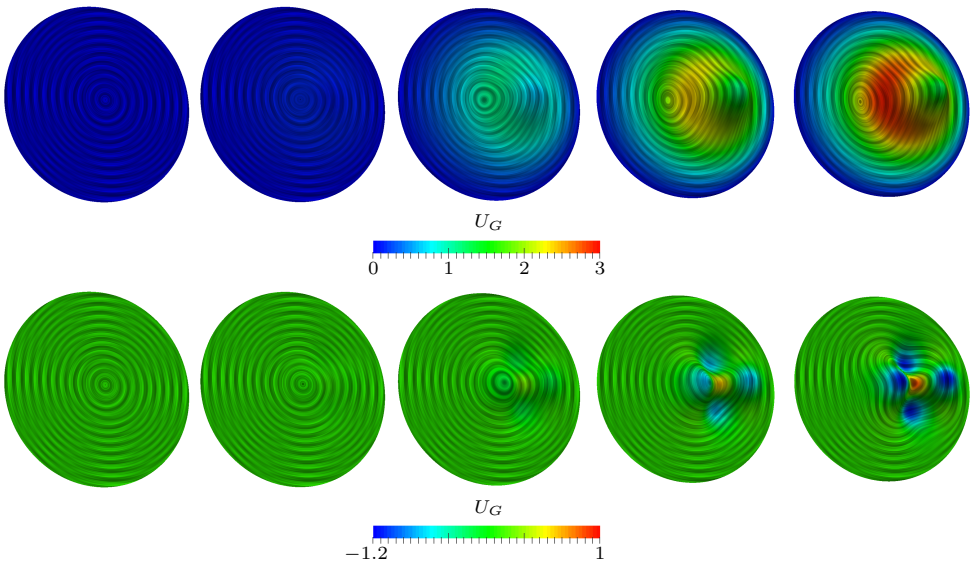

FIG. 4. *Time evolution of* $\mathbf{v}$ *for the bump and the Gaussian saddle for* $t = 2, 14, 26, 38,$ *and* 50 *visualized as a noise concentration field aligned to the velocity field* $\mathbf{v}$. *The color coding is according to the geometric potential* U_G.

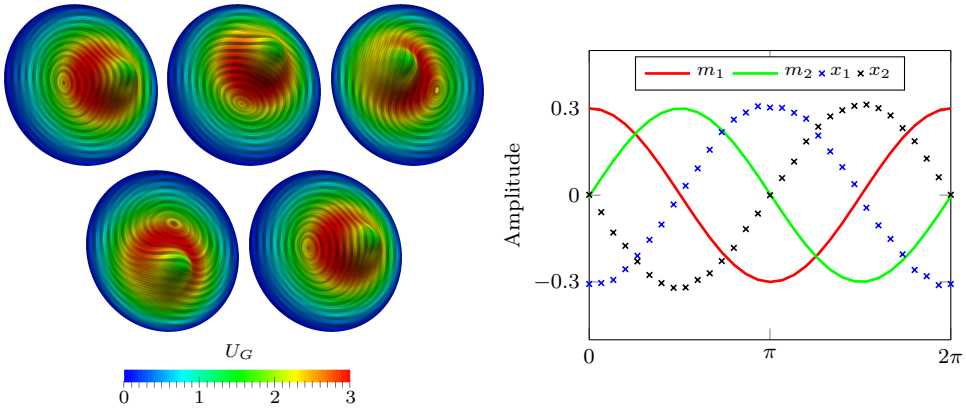

FIG. 5. *Time evolution of* $\mathbf{v}$ *for the bump for* $t = 2, 11, 19, 27$, *and* 36 *(left to right and top to bottom) visualized as a noise concentration field aligned to the velocity field* $\mathbf{v}$ *(left) and evolution of the bump location* $(m_1, m_2)^T$ *and the vortex location* $(x_1, x_2)^T$ *for a full period of rotation (right). The color coding is according to the geometric potential* U_G.

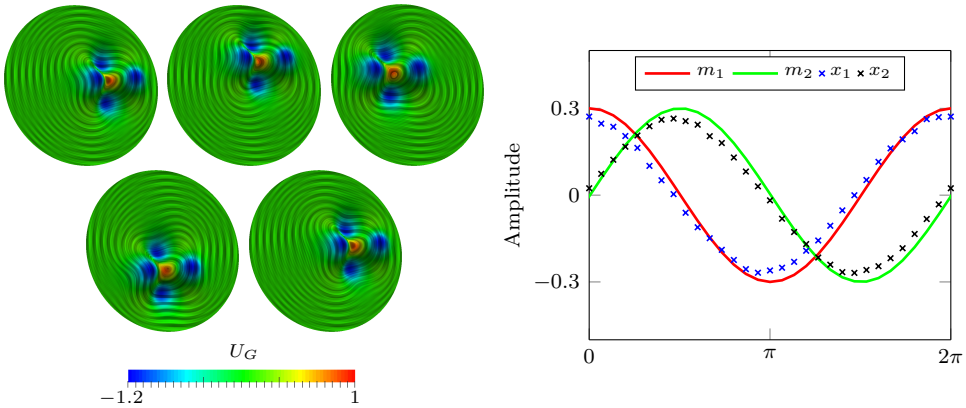

FIG. 6. *Time evolution of* $\mathbf{v}$ *for the Gaussian saddle for* $t = 2, 11, 19, 27$, *and* 36 *(left to right and top to bottom) visualized as a noise concentration field aligned to the velocity field* $\mathbf{v}$ *(left) and evolution of the bump location* $(m_1, m_2)^T$ *and the vortex location* $(x_1, x_2)^T$ *for a full period of rotation (right). The color coding is according to the geometric potential* U_G.

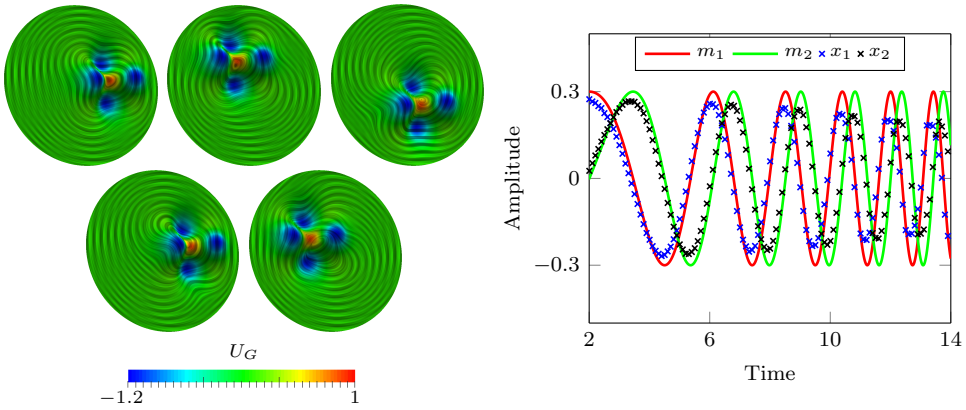

FIG. 7. *Time evolution of* $\mathbf{v}$ *for the accelerated rotation of the Gaussian saddle for* $t = 2, 7, 10, 12,$ *and* 14 *(left to right and top to bottom) visualized as a noise concentration field aligned to the velocity field* $\mathbf{v}$ *(left) and time evolution of the Gaussian saddle location* $(m_1, m_2)^T$ *and the vortex location* $(x_1, x_2)^T$ *(right). The color coding is according to the geometric potential* U_G.

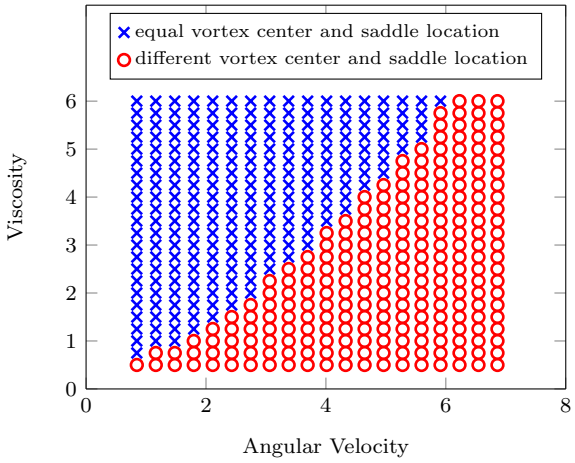

FIG. 8. *Viscosity versus angular velocity phase diagram. Here it is assumed that the vortex is placed off the Gaussian saddle if* $||(m_1, m_2)^T - (x_1, x_2)^T|| \geq 0.075$ *(red circles). Blue crosses indicate high geometric influences through vortex trapping.*

REFERENCES

[1] M. Arroyo and A. DeSimone, *Relaxation dynamics of fluid membranes*, Phys. Rev. E, 79 (2009), 031915, https://doi.org/10.1103/PhysRevE.79.031915.

[2] T. Jankuhn, M. A. Olshanskii, and A. Reusken, *Incompressible Fluid Problems on Embedded Surfaces: Modeling and Variational Formulations*, arXiv:1702.02989, 2017.

[3] H. Koba, C. Liu, and Y. Giga, *Energetic variational approaches for incompressible fluid systems on an evolving surface*, Quart. Appl. Math., 75 (2017), pp. 359–389, https://doi.org/10.1090/qam/1452.

[4] T.-H. Miura, *On Singular Limit Equations for Incompressible Fluids in Moving Thin Domains*, arXiv:1703.09698, 2017.

[5] I. Nitschke, A. Voigt, and J. Wensch, *A finite element approach to incompressible two-phase flow on manifolds*, J. Fluid Mech., 708 (2012), pp. 418–438.

[6] S. Reuther and A. Voigt, *The interplay of curvature and vortices in flow on curved surfaces*, Multiscale Model. Simul., 13 (2015), pp. 632–643, https://doi.org/10.1137/140971798.
[7] S. Vey and A. Voigt, *AMDiS: Adaptive multidimensional simulations*, Comput. Vis. Sci., 10 (2007), pp. 57–67.
[8] T. Witkowski, S. Ling, S. Praetorius, and A. Voigt, *Software concepts and numerical algorithms for a scalable adaptive parallel finite element method*, Adv. Comput. Math., 41 (2015), pp. 1145–1177.
[9] A. Yavari, A. Ozakin, and S. Sadik, *Nonlinear elasticity in a deforming ambient space*, J. Nonlinear Sci., 26 (2016), pp. 1651–1692, https://doi.org/10.1007/s00332-016-9315-8.